

RESEARCH ARTICLE

A reaction-diffusion type mathematical model for the formation of coral patterns

L.W. Somathilake^{1*} and J.R. Wedagedera²

¹ Department of Mathematics, Faculty of Science, University of Ruhuna, Matara.

² Simcyp-CERTARA Limited, Blades Enterprise Centre, John Street, Sheffield S2 4SU, United Kingdom.

Revised: 07 April 2014; Accepted: 18 July 2014

Abstract: A reaction-diffusion type mathematical model for the growth of corals in a tank has been proposed based on the model suggested by Mistr and Bercovici, emphasizing the effect of nutrient concentration and domain size on growth patterns. The Turing type pattern formation of the proposed model has been considered and the pattern formation parameter spaces (Turing spaces) of the model were determined. The model is solved numerically when the parameters lie in Turing space and the results are represented graphically. These numerical solutions resemble branching structures of some branching corals. It has been observed that the behaviour of the branching structures vary with parameter values as well as the considered domain size (dimensions of the tank).

Keywords: Pattern formation, reaction-diffusion equations, spatial temporal, Turing instability.

INTRODUCTION

Corals are made up of a vast amount of calcium carbonate deposited by the colonies of cnidarian polyps. These colonies are formed when a planktonic coral larvae, called a planulae, settles on a hard surface. The larvae transforms itself into a polyp just after settling (Castro & Huber, 1997). The maximum diameter of a polyp is a species-specific characteristic. Once they reach this maximum diameter they divide recurrently and form a colony (Merks *et al.*, 2003b). If the coral colony does not break off, it grows intensively as its individual polyps divide to form new polyps (Castro & Huber, 1997). In stony corals the polyps reside in cup like skeletal structures called the calices (Merks *et al.*, 2003b). As new polyps are formed they build new calices. This causes the growth of the solid matrix of stony corals.

Different aspects of coral morphogenesis have been studied using various modelling and computational approaches (Kaandorp *et al.*, 1996; 2005; 2008; Merks, 2003; Merks *et al.*, 2003a;b; Filatov *et al.*, 2010) and some fascinating stony coral simulations have been reported (Merks, 2003; Merks *et al.*, 2003a; b; Kaandorp *et al.*, 2005; 2008; Filatov *et al.*, 2010). A reaction-diffusion-advection type model for the growth of corals has been proposed by Mistr and Bercovici (2003).

The morphogenesis of branching corals have been described by the diffusion-limited aggregation (DLA) type models and the patterns generated by this method for stony corals have been recorded (Merks 2003; Merks *et al.*, 2003b; c).

The objective of this paper is to propose a reaction-diffusion type mathematical model for the formation of coral patterns, emphasizing the effect of nutrient concentration and the domain size. It is assumed that all the other factors that affect the growth of coral are fixed.

METHODOLOGY

A reaction-diffusion type mathematical model

A water filled tank with some coral larvae (planulae) settled on the bottom of the tank was considered. It was assumed that the nutrients are supplied to the tank at a rate u_3 at the top surface of the tank. It was also assumed that the growth factors except the availability of nutrients are fixed.

* Corresponding author (sthilake@maths.ruh.ac.lk)

The coral polyps consume dissolved nutrients and produce additional solid material (corals produce their skeleton by extracting dissolved calcium carbonate surrounding them). This process can be regarded as a reaction process between the dissolved nutrients and the dissolved calcium carbonate. Let A and B denote the dissolved nutrients and the dissolved solid material (calcium carbonate) respectively. This process can be expressed as a hypothetical reaction between A and B of the form (Mistr & Bercovici, 2003):



where k is a positive rate constant (reaction rate). l, m and n are the respective stoichiometric constants such that $n = m + l$. Units of k depend on the stoichiometric constants l, m and n . Then by the law of mass action (Murray, 2003) we have the rate change of solid material, which is proportional to uv^m . Mistr and Bercovici (2003) investigated the stability of the system for various m and found that the system is unstable yielding solid growth only in cases where $m \geq 2$. They have used the lowest order unstable case ($l = 1, m = 2$) and the same case has been used in this paper.

Let $u \equiv u(x, y, z, t)$ and $v \equiv v(x, y, z, t)$ be the biomass of dissolved nutrient and calcium carbonate ions at the point $(x, y, z) \in \Omega$ at time $t(> 0)$. Here Ω is the considered model geometry (geometry of the tank). The time rate of change of the nutrient concentration is controlled by diffusion and reactive loss of nutrients. We can immediately write the rate equation for this process by applying the law of mass action and Fick's law, as follows:

$$\frac{\partial u}{\partial t} = D_u \nabla^2 u - kuv^2 \quad \dots(2)$$

The time rate of change of the solid material is controlled by diffusion, loss due to deposition and reactive production. Assume that the polyps extract the dissolved calcium carbonate at the rate $k_1(> 0)$. That is the solid materials deposit on the existing solid matrix (coral particles) at the rate k_1 . Then the rate equation of this process is:

$$\frac{\partial v}{\partial t} = D_v \nabla^2 v - k_1 v + kuv^2 \quad \dots(3)$$

$D_u(> 0)$ and $D_v(> 0)$ in above equations are the diffusion rates of dissolved nutrients and the calcium carbonate ions, respectively. Let C denote the solid material deposited by coral polyps and w denote its biomass. This process can be symbolized as follows.

$$\frac{\partial w}{\partial t} = k_1 v \quad \dots(4)$$

We now have the following set of governing equations for the process:

$$\left. \begin{aligned} \frac{\partial u}{\partial t} &= D_u \nabla^2 u - kuv^2, \quad x \in \Omega \subset \mathbb{R}^3, \quad t > 0, \\ \frac{\partial v}{\partial t} &= D_v \nabla^2 v - k_1 v + kuv^2, \quad x \in \Omega \subset \mathbb{R}^3, \\ \frac{\partial w}{\partial t} &= k_1 v, \quad x \in \Omega \subset \mathbb{R}^3, \quad t > 0. \end{aligned} \right\} \quad \dots(5)$$

Simplification to a two-dimensional model and nondimensionalization

Assume that the nutrients are supplied at the top surface at a fixed rate u_s . That is $u = u_s$ at $z = H$ where H is the depth of the considered tank. We assume that u and v vary from top to bottom of the considered tank as follows (Mistr & Bercovici, 2003):

$$v(x, y, z, t) = \bar{v}(x, y, t)f(z), \quad \dots(6)$$

$$u(x, y, z, t) = u_s + (\bar{u}(x, y, t) - u_s)f(z) \text{ and} \quad \dots(7)$$

$$w(x, y, z, t) = \bar{w}(x, y, t)f(z), \quad \dots(8)$$

where

$$f(z) = \frac{3}{2} \left(1 - \frac{z^2}{H^2} \right) \quad \dots(9)$$

Since $\frac{1}{H} \int_0^H f(z) dz = 1$, \bar{u} and \bar{v} are the averaged values of u and v over z . Assume that $\frac{1}{H} \int_0^H f^m(z) dz \simeq 1$ for $m = 1, 2, 3$. Substituting the above values in the governing equations (5) and integrating over z we get

$$\left. \begin{aligned} \frac{\partial \bar{u}}{\partial t} &= D_u \nabla_h^2 \bar{u} + D_u \frac{3(u_s - \bar{u})}{H^2} - k\bar{v}^2 \bar{u}, \\ \frac{\partial \bar{v}}{\partial t} &= D_v \nabla_h^2 \bar{v} - D_v \frac{3\bar{v}}{H^2} - k_1 \bar{v} + k\bar{v}^2 \bar{u}, \\ \frac{\partial \bar{w}}{\partial t} &= k_1 \bar{v}, \end{aligned} \right\} \quad \dots(10)$$

where $\nabla_h^2 = \frac{\partial^2}{\partial x^2} + \frac{\partial^2}{\partial y^2}$ is the horizontal Laplace operator.

Substitute $\hat{u} = u_s \bar{u}$, $\hat{v} = u_s \bar{v}$, $\hat{w} = u_s \bar{w}$, $\hat{x} = \frac{\sqrt{3}}{H} x$, $\hat{y} = \frac{\sqrt{3}}{H} y$. Then the system reduce to:

$$\left. \begin{aligned} u_s \frac{\partial \hat{u}}{\partial t} &= \frac{3D_u u_s}{H^2} \hat{\nabla}_h^2 \hat{u} + \frac{3D_u}{H^2} (u_s - u_s \hat{u}) - u_s^3 \hat{v}^2 \hat{u} \\ u_s \frac{\partial \hat{v}}{\partial t} &= \frac{3D_v u_s}{H^2} \hat{\nabla}_h^2 \hat{v} - \frac{3D_v u_s}{H^2} \hat{v} - k_1 u_s \hat{v} + u_s^3 \hat{v}^2 \hat{u} \\ u_s \frac{\partial \hat{w}}{\partial t} &= k_1 u_s \hat{v}, \end{aligned} \right\} \quad \dots(11)$$

where $\hat{\nabla}^2 = \frac{\partial^2}{\partial \hat{x}^2} + \frac{\partial^2}{\partial \hat{y}^2}$.

Substituting $\hat{t} = \frac{3D_u}{H^2}t$, the system can be reduced to:

$$\left. \begin{aligned} \frac{\partial \hat{u}}{\partial \hat{t}} &= \hat{\nabla}_h^2 \hat{u} + 1 - \hat{u} - \alpha^2 \hat{v}^2 \hat{u} \\ \frac{\partial \hat{v}}{\partial \hat{t}} &= d \hat{\nabla}_h^2 \hat{v} - \lambda \hat{v} + \alpha^2 \hat{v}^2 \hat{u}, \\ \frac{\partial \hat{w}}{\partial \hat{t}} &= \lambda_1 \hat{v}, \end{aligned} \right\} \dots(12)$$

where $d = \frac{D_v}{D_u}$, $\alpha^2 = \frac{kH^2u_s^2}{3D_u}$, $\lambda = d + \frac{k_1H^2}{3D_u}$ and $\lambda_1 = \frac{k_1H^2}{3D_u}$. For the notational convenience we omit

the hats of the above two equations. Then the model equation is:

$$\left. \begin{aligned} \frac{\partial u}{\partial t} &= \nabla^2 u + 1 - u - \alpha^2 v^2 u, \quad x \in \Omega \subset \mathbb{R}^2, \quad t > 0 \\ \frac{\partial v}{\partial t} &= d \nabla^2 v - \lambda v + \alpha^2 v^2 u, \quad x \in \Omega \subset \mathbb{R}^2, \quad t > 0 \\ \frac{\partial w}{\partial t} &= \lambda_1 v, \quad x \in \Omega \subset \mathbb{R}^2, \quad t > 0. \end{aligned} \right\} \dots(13)$$

Turing instability of the model

Some reaction diffusion systems have a special characteristic of having stable steady states in the absence of diffusion (in a spatially homogeneous system), and these states become unstable in the presence of diffusion (in a spatially inhomogeneous system). Solutions of such systems form spatial temporal patterns. By imposing these conditions for a reaction diffusion system some conditions can be derived in terms of model parameters. That means the reaction diffusion systems may form spatial patterns when satisfying these conditions. In 1952, the mathematician Alan Turing explained this phenomena for reaction diffusion systems in chemistry (Turing, 1952) and hence these conditions are called Turings instability conditions. In Murray (2003), the Turing instability conditions for the general forms

$$\left. \begin{aligned} \frac{\partial u}{\partial t} &= \nabla^2 u + F(u, v), \quad x \in \Omega \subset \mathbb{R}^2, \quad t > 0 \\ \frac{\partial v}{\partial t} &= d \nabla^2 v + G(u, v), \quad x \in \Omega \subset \mathbb{R}^2, \quad t > 0 \end{aligned} \right\}$$

have been derived subject to no-flux boundary conditions. These conditions take the form:

$$\begin{aligned} (TC_1) &\equiv \text{Det}(A) > 0, \\ (TC_2) &\equiv \text{Tr}(A) < 0, \\ (TC_3) &\equiv d(a_{11}) + (a_{22}) > 0, \\ (TC_4) &\equiv (TC_3)^2 - 4d(TC_1) > 0; \end{aligned}$$

where

$$A = \left(\begin{array}{cc} F_u & F_v \\ G_u & G_v \end{array} \right) \Big|_S = \left(\begin{array}{cc} a_{11} & a_{12} \\ a_{21} & a_{22} \end{array} \right) \Big|_S$$

and $s \equiv (u_0, v_0)$ is a stable steady state of the corresponding spatially homogeneous system.

This section investigates the parameter regions in which the Turing instability conditions are satisfied (Turing instability region) by the reaction-diffusion system (equation 13) under the no-flux boundary conditions:

$$\left. \begin{aligned} \nabla u \cdot \mathbf{n} &= 0, \quad x \in \partial\Omega, \\ \nabla v \cdot \mathbf{n} &= 0, \quad x \in \partial\Omega, \end{aligned} \right\} \dots(14)$$

where ∇ denotes the gradient operator and \mathbf{n} denotes the outward unit normal vector to the domain boundary $\partial\Omega$.

Steady states

There are three homogeneous steady sates $S_1 \equiv (u_{s1}, v_{s1})$, $S_2 \equiv (u_{s2}, v_{s2})$ and $S_3 \equiv (u_{s3}, v_{s3})$ for the corresponding system of ordinary differential

equations. Here $u_{s1} = 1, v_{s1} = 0, u_{s2} = \frac{\alpha - \sqrt{\alpha^2 - 4\lambda^2}}{2\alpha}$,
 $v_{s2} = \frac{\alpha + \sqrt{\alpha^2 - 4\lambda^2}}{2\alpha\lambda}, u_{s3} = \frac{\alpha + \sqrt{\alpha^2 - 4\lambda^2}}{2\alpha}$ and $v_{s3} = \frac{\alpha - \sqrt{\alpha^2 - 4\lambda^2}}{2\alpha\lambda}$ for $\alpha > 2\lambda$.

The Jacobian matrix evaluated at S_i is:

$$A_i = \left(\begin{array}{cc} F_u & F_v \\ G_u & G_v \end{array} \right) \Big|_{S_i} = \left(\begin{array}{cc} a_{11} & a_{12} \\ a_{21} & a_{22} \end{array} \right) \Big|_{S_i} = \left(\begin{array}{cc} -1 - \alpha^2 v_{si}^2 & -2\lambda \\ \alpha^2 v_{si}^2 & \lambda \end{array} \right) \dots(15)$$

where $F(u, v) = 1 - u - \alpha^2 uv^2$ and $G(u, v) = -\lambda v - \alpha^2 uv^2$. The trace and determinant of A_i are $Tr(A_i) = \lambda - 1 - \alpha^2 v_{si}^2$ and $Det(A_i) = \lambda(\alpha^2 v_{si}^2 - 1)$, respectively.

RESULTS AND DISCUSSION

Turing instability conditions

The Turing instability conditions at the steady state S_i take the form:

$$\begin{aligned}
 (TC_1)_i \equiv \text{Det}(A_i) > 0, & \Rightarrow \lambda(\alpha^2 v_{si}^2 - 1) > 0, \\
 (TC_2)_i \equiv \text{Tr}(A_i) < 0, & \Rightarrow \lambda - (1 + \alpha^2 v_{si}^2) < 0, \\
 (TC_3)_i \equiv d(a_{11})_i + (a_{22})_i > 0, & \Rightarrow \lambda - d(1 + \alpha^2 v_{si}^2) > 0, \\
 (TC_4)_i \equiv (TC_3)_i^2 - 4d(TC_1)_i > 0; & \Rightarrow (d(1 + \alpha^2 v_{si}^2) - \lambda)^2 \\
 & - 4d\lambda(\alpha^2 v_{si}^2 - 1) > 0.
 \end{aligned}
 \dots(16)$$

Consider the case $\alpha > 2\lambda$. It can be shown that the trivial steady state S_1 is a stable node, S_3 is a saddle point and the stability of S_2 further depends on the values of the parameters α and λ . It can be shown that the above conditions are not satisfied at S_1 . Since S_3 is a saddle point, the Turing instability does not occur at S_3 . Therefore, the Turing type instability may occur only at S_2 and this paper considers the Turing type patterns at S_2 . The Turing conditions at S_2 are $(TC_i)_2, i = 1, 2, 3, 4$. For the notational convenience, ignore the index 2 of $(TC_i)_2$. The Turing instability conditions at S_2 can be obtained in the following form by substituting v_{s2} in terms of model parameters, in the inequalities (equation 16).

$$TC_1 \equiv \frac{\alpha^2 - 4\lambda^2 + \alpha\sqrt{\alpha^2 - 4\lambda^2}}{2\lambda} > 0,$$

$$TC_2 \equiv -\frac{\alpha^2 - 2\lambda^3 + \alpha\sqrt{\alpha^2 - 4\lambda^2}}{2\lambda^2} < 0,$$

$$TC_3 \equiv \frac{2\lambda^3 - \alpha d(\alpha + \sqrt{\alpha^2 - 4\lambda^2})}{2\lambda^2} > 0,$$

$$TC_4 \equiv \left(\frac{2\lambda^3 - d\alpha(\alpha + \sqrt{\alpha^2 - 4\lambda^2})}{2\lambda^2}\right)^2 - 4d\left(\frac{\alpha^2 - 4\lambda^2 + \alpha\sqrt{\alpha^2 - 4\lambda^2}}{2\lambda}\right) > 0.$$

It can be shown that TC_1 is held at S_2 in the region $\alpha > 2\lambda$. Therefore only TC_2, TC_3 and TC_4 are checked. The bifurcation $TC_2 = 0$ (Hopf bifurcation), gives two real roots for when $\lambda > 1$. These are

$$(TC_2)\alpha_{1,2} = \frac{\pm\lambda^2}{\sqrt{\lambda-1}}$$

The equation $TC_3 = 0$ gives two real roots for α when $\lambda > d$. These are

$$(TC_3)\alpha_{1,2} = \frac{\pm\lambda^2}{\sqrt{d(\lambda-d)}}$$

The equation $TC_4 = 0$ gives four real roots for α when $\lambda > d$. Among these roots two are positive. These positive roots are:

$$(TC_4)\alpha_{1,2} = \frac{\sqrt{d\lambda^3(8d^2 + 7d\lambda + 3\lambda^2) \mp 2\sqrt{2}d\sqrt{\lambda^7(\lambda-d)(2d+\lambda)^2}}}{d(d+\lambda)}$$

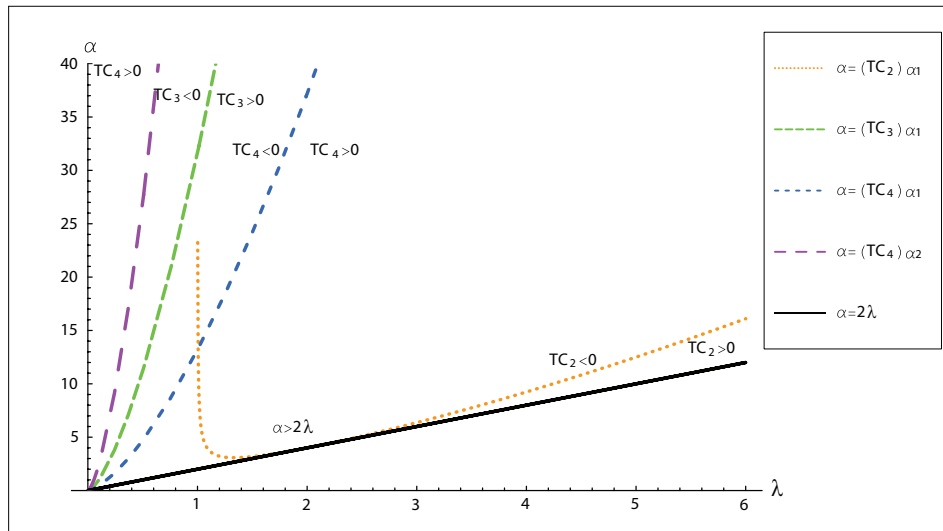


Figure 1: Curves to determine Turing space for $d = 0.001$

Figure 1 shows the plots of $\alpha = (TC_2)\alpha_1, \alpha = (TC_3)\alpha_2$ and $\alpha = (TC_4)\alpha_{1,2}$ for $d = 0.001$.

Since $\alpha > 2\lambda$ putting $\alpha = 2\lambda + \epsilon (\epsilon > 0)$ in TC_2 , we have

$$\begin{aligned}
 TC_2 &= -\frac{(2\lambda + \epsilon)^2 - 2\lambda^3 + (\text{positive term})}{2\lambda^2} \\
 &= -\frac{2\lambda^2(2 - \lambda) + (\text{positive term})}{2\lambda^2} \\
 &< 0; \text{ if } \lambda < 2.
 \end{aligned}
 \dots(17)$$

Therefore TC_2 is negative for $\lambda < 2$. Also, $(TC_3)\alpha_1 > [(TC_4)\alpha_1]$ for $\lambda \neq 2d$ and $(TC_3)\alpha_1 = (TC_4)\alpha_1$ for $\alpha = 2d$.

Moreover

$$TC_3 = -\frac{d(2\lambda + \epsilon)^2 - 2\lambda^3 + (\text{positive term})}{2\lambda^2}$$

$$= -\frac{2\lambda^2(2d - \lambda) + (\text{positive term})}{2\lambda^2}$$

< 0 ; if $\lambda < 2d$(18)

Therefore TC_3 is not satisfied in the region $\lambda < 2d$. By considering these facts, the instability region (Turing space) can be written as a union of two regions \mathcal{R}_1 and \mathcal{R}_2 .

Where,

\mathcal{R}_1 : The area covered by the line $\alpha = 2\lambda$ and the curve $\alpha = (TC_4)\alpha_1$ for $\lambda \leq 2$. That is

$$\mathcal{R}_1 = \{(\lambda, \alpha); \quad 2d \leq \lambda \leq 2, \quad 2\lambda < \alpha < (TC_4)\alpha_1\}$$

\mathcal{R}_2 : The area covered by the curves $\alpha = (TC_2)\alpha_1$ and $\alpha = (TC_4)\alpha_1$ for $\lambda > 2$. That is

$$\mathcal{R}_2 = \{(\lambda, \alpha); \quad \lambda > 2, \quad (TC_2)\alpha_1 < \alpha < (TC_4)\alpha_1\}$$

Now we consider the points of intersection of the curves $\alpha = (TC_2)\alpha_1$ and $\alpha = (TC_4)\alpha_1$. These curves intersect at two points (say $\lambda = \lambda_1$, $\lambda = \lambda_2$). Here

$$\lambda_1 = \frac{-8d}{1 - 6d + d^2}$$

$$\lambda_2 = \frac{2}{3}(1 - d) + \frac{d^2 + 22d + 1}{3(d^3 - 75d^2 - 33d - 1 + 6\sqrt{6d}\sqrt{19d^2 - 27d - d^3 - 1})^{1/3}}$$

$$+ \frac{1}{3}(d^3 - 75d^2 - 33d - 1 + 6\sqrt{6d}\sqrt{19d^2 - 27d - d^3 - 1})^{1/3}.$$

λ_1 has an asymptote when $d^2 - 6d + 1 = 0$. That is λ_1 has an asymptote at $d = d_{c1} = 3 \pm 2\sqrt{2}$.

The plots of λ_1 and λ_2 with respect to d are shown in Figure 2. When $d = 1$, λ_1 and λ_2 coincide each other. That is when $d = 1$, the area covered by the curves $\alpha = (TC_2)\alpha_1$ and $\alpha = (TC_4)\alpha_1$ vanishes. That is when $d = 1$ the Turing space vanishes.

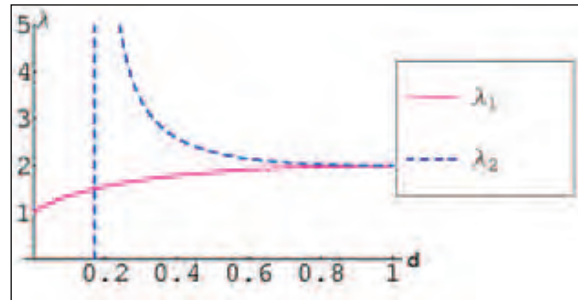


Figure 2: λ_1 and λ_2 curves with respect to d

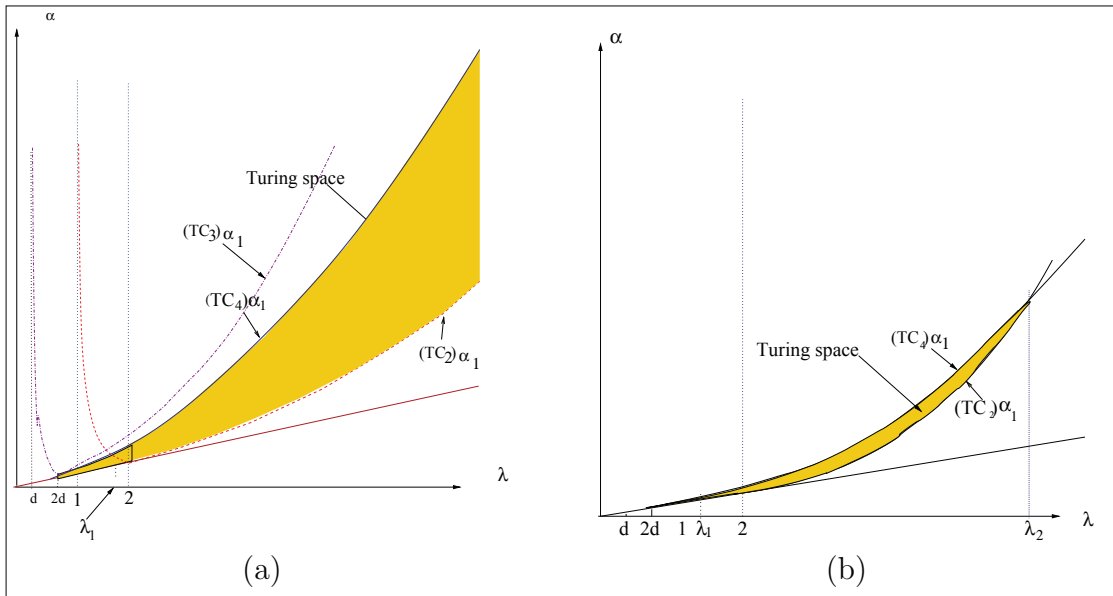


Figure 3: Sketches of Turing space: (a) $d < d_{c1}$; (b) $d > d_{c1}$. In each figure dashed curve is $\alpha = (TC_4)\alpha_1$, solid curve is $\alpha = (TC_2)\alpha_1$ and the straight line is $\alpha = 2\lambda$. Shaded area is the Turing space.

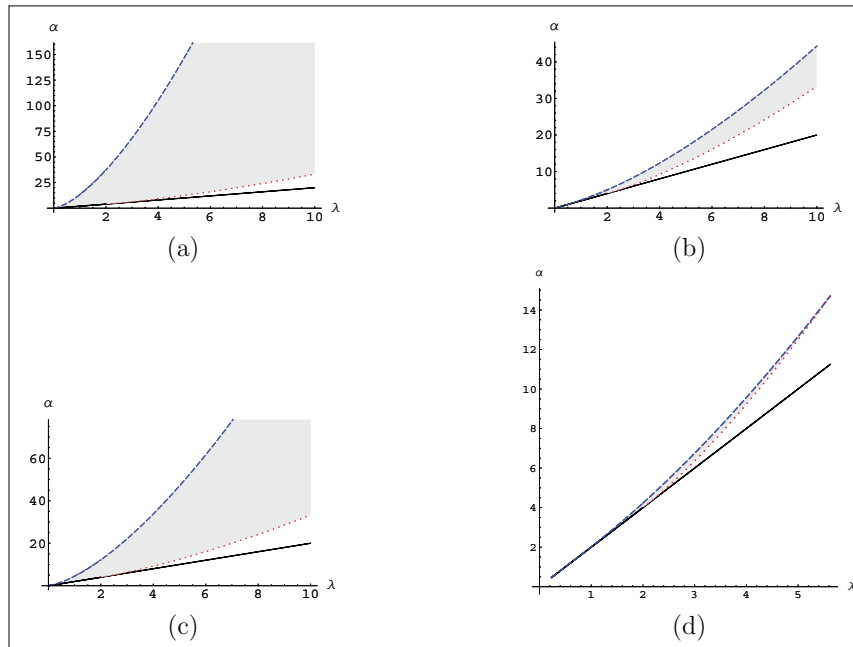


Figure 4: (λ, α) parameter space (shaded area) for different values of d : (a) $d = 0.001$; (b) $d = 0.1$; (c) $d = 0.01$ and (d) $d = 0.23$. In each figure, upper curve (dashed curve): $\alpha = (TC_4)\alpha_1$; middle curve (dotted curve): $\alpha = (TC_2)\alpha_1$ and lower line (solid line): $\alpha = 2\lambda$

When $d < d_{c1}$ the curves $\alpha = (TC_2)\alpha_1$ and $\alpha = (TC_4)\alpha_1$ intersect only at one point ($\lambda = \lambda_1 < 2$) and these curves intersect at two points ($\lambda = \lambda_1$ and $\lambda = \lambda_2$) when $d > d_{c1}$ in the range of positive λ . This behaviour and the Turing spaces corresponding to two points in the ranges $0 < d < d_{c1}$ and $d_{c1} < d < 1$ are sketched in Figure 3. The (α, λ) parameter spaces (Turing spaces) for different values of d are shown in Figure 4.

Numerical results

Coral reefs grow due to the deposition of calcium carbonate on existing reefs. In equation 13, w represents the vertically averaged nondimensionalized depositing amount of solid materials on the coral reef. From the equation 13 we get:

$$w(x, y, t) = \int_0^t k_1 v(x, y, \tau) d\tau$$

The density v at time t is proportional to the aggregating amount of the solid material at time t . In other words the density plot of v gives some information on overall aggregating amount w . Consider the one dimensional case of the equations 13-14:

$$\left. \begin{aligned} \frac{\partial u}{\partial t} &= \frac{\partial^2 u}{\partial x^2} + 1 - u - \alpha^2 v^2 u, & x \in \Omega, & t > 0 \\ \frac{\partial v}{\partial t} &= d \frac{\partial^2 v}{\partial x^2} - \lambda v + \alpha^2 v^2 u, & x \in \Omega, & t > 0 \end{aligned} \right\} \dots(19)$$

with the boundary conditions

$$\left. \begin{aligned} \frac{\partial u}{\partial x} &= 0, & x \in \partial\Omega, \\ \frac{\partial v}{\partial x} &= 0, & x \in \partial\Omega \end{aligned} \right\} \dots(20)$$

where $\Omega = (0, L)$.

This system is solved with MATLAB pdepe (MathWorks, 2014a) solver under the initial state:

$$u(x, 0) = u_{02} \quad x \in \Omega, \\ v(x, 0) = \begin{cases} v_{02} + v_{02} \frac{\text{Rand}[0, 1]}{100}, & x \in \omega \\ v_{02}, & x \in \Omega \setminus \omega. \end{cases} \dots(21)$$

Here $\omega = \left(\frac{L}{2} - \frac{L}{100}, \frac{L}{2} + \frac{L}{100} \right)$.

In these simulations the error control options AbsTol and RelTol were kept in their default values, RelTol= 10^{-3} and AbsTol= 10^{-6} .

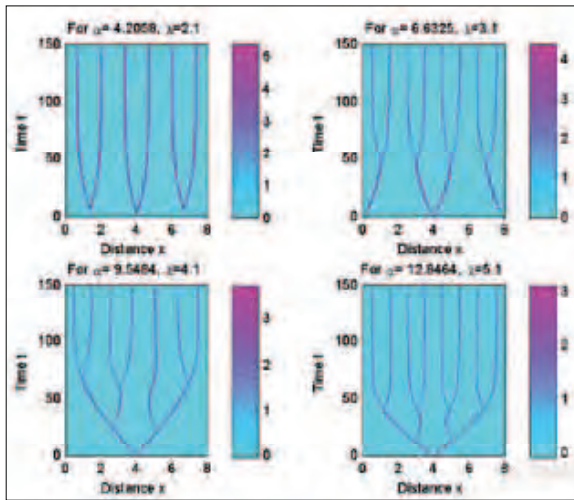


Figure 5: Density plot of $v(x, t)$ for different values of α and λ

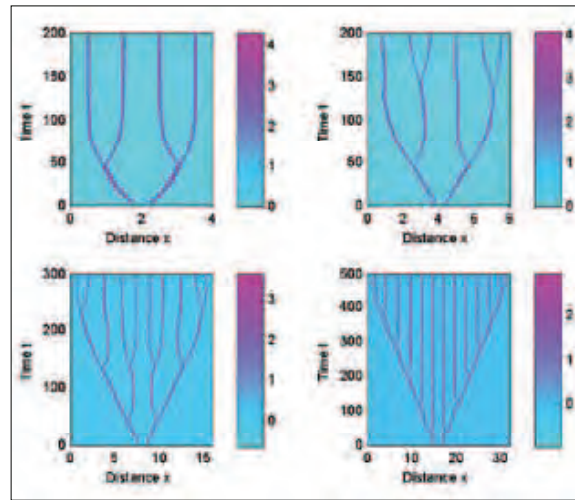


Figure 6: Density plot of $v(x, t)$ for different domain sizes

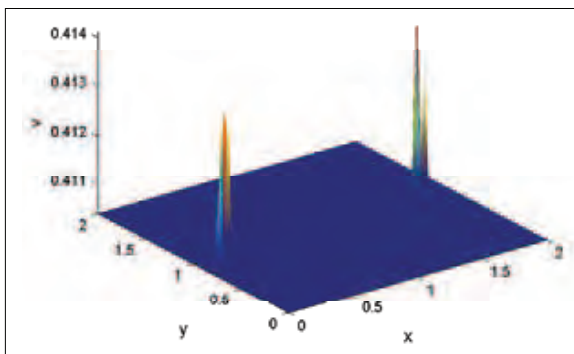


Figure 7: Initial state $v(x, y, 0)$

The density plots of $v(x, t)$ for different values of parameters (α and λ), are shown in Figure 5. Accordingly the heterogeneity of the space patterns is increased as α increases from its critical value by keeping λ fixed.

Figure 6 exhibits the density plots of $v(x, t)$ when $\lambda = 3.2$ and $\alpha = 6.48596$ for different domain sizes. These figures show that the heterogeneity of the spatial patterns increases as domain size increases for fixed parameter values.

Also, the reaction diffusion system is solved numerically on 2D domain, $\Omega \equiv [0, 2] \times [0, 2]$, subject to no-flux

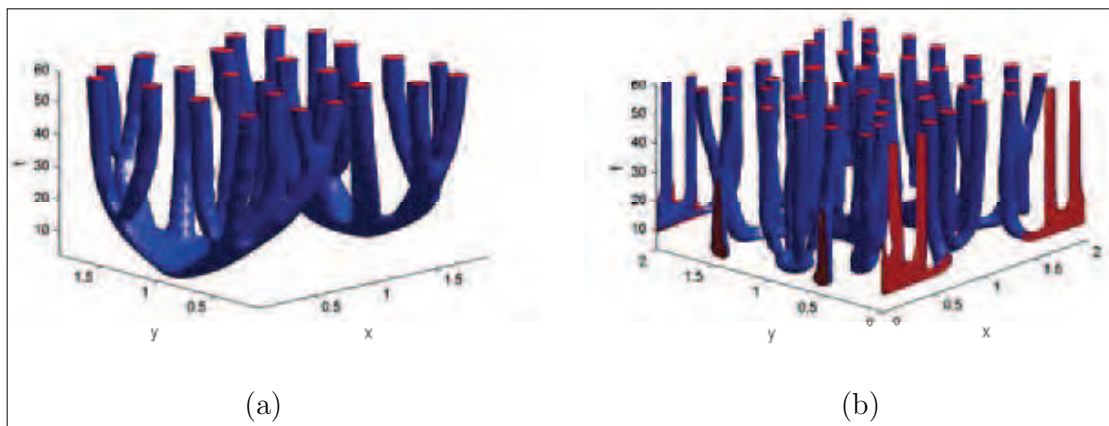


Figure 8: Isosurfaces of numerical solutions of $v(x, y, t)$ for some parameter values. (a) $\lambda = 2.3, \alpha = 5$; (b) $\lambda = 2.3, \alpha = 10$

boundary conditions. The considered initial state is as follows:

$$\begin{aligned} u(x, y, 0) &= u_{02} \quad (x, y) \in \Omega, \\ v(x, y, 0) &= \begin{cases} v_{02} + v_{02} \frac{\mathbf{Rand}[0, 1]}{100}, & (x, y) \in \omega \\ v_{02}, & (x, y) \in \Omega \setminus \omega. \end{cases} \end{aligned} \quad \dots(22)$$

Here ω is the union of the circular region with center (1/4, 1), radius 1/25 and the circular region with center (7/4, 1), radius 1/25 (Figure 7).

In these numerical simulations the following very standard semi-implicit finite difference scheme is used.

$$\begin{aligned} \frac{u_{i,j}^{n+1} - u_{i,j}^n}{k} &= \frac{u_{i+1,j}^{n+1} + u_{i-1,j}^{n+1} + u_{i,j+1}^{n+1} + u_{i,j-1}^{n+1} - 4u_{i,j}^{n+1}}{h^2} + F(u_{i,j}^n, v_{i,j}^n), \\ \frac{v_{i,j}^{n+1} - v_{i,j}^n}{k} &= d \frac{v_{i+1,j}^{n+1} + v_{i-1,j}^{n+1} + v_{i,j+1}^{n+1} + v_{i,j-1}^{n+1} - 4v_{i,j}^{n+1}}{h^2} + G(u_{i,j}^n, v_{i,j}^n). \end{aligned}$$

Here $F(u, v) = 1 - u - \alpha^2 uv^2$, $G(u, v) = -\lambda v + \alpha^2 uv^2$. k is step size of time and h is the step size of x and y directions of the domain. The linear system, arisen after applying a finite difference technique, is solved using the conjugate gradient iterative method. The termination of this iterative methods was controlled by applying a tolerance for the relative error. This tolerance was taken as 10^{-15} . Isosurfaces of numerically evaluated $v(x, y, t)$ for different parameter vales are shown in Figures 8. These isosurfaces were obtained by plotting the numerically evaluated $v(x, y, t)$ using MATLAB built in functions isosurface (MathWorks, 2014b) and isocaps (MathWorks, 2014c).

CONCLUSION

There are three spatially homogeneous steady states S_1 , S_2 , S_3 for the model. The Turing instability conditions are satisfied at S_2 for particular parameter values and the Turing space for the same (the parameter space at which the Turing instability conditions are satisfied) was determined.

It was observed that the area of the Turing space decreases as d increases from 0 to 1 and it disappears when $d = 1$. In other words the diffusion rate of the dissolved solid material should be less than that of dissolved nutrient in order for Turing instability to occur. There is a critical value d_{c1} for the diffusion rate d at which the Turing space divides into two forms, confined region (bounded region) and unconfined region (unbounded region), (Figure 3).

The parameters d , α and λ of the proposed model are defined as $d = \frac{D_v}{D_u}$, $\alpha^2 = \frac{kH^2 u_s^2}{3D_u}$ and $\lambda = d + \frac{k_1 H^2}{3D_u}$. Turing type patterns are possible if these parameters lie in the Turing instability region. Considering the case of growing corals in a tank, if we assume that the growth factors of coral are fixed except the nutrient availability, it is reasonable to assume that D_u , D_v , H , k and k_1 are fixed in this case. Then λ and d are fixed and α depend on the nutrient supplying rate u_s . By adjusting the nutrient supplying rate one can adjust α such that all parameters lie in the Turing instability region. Then spatial temporal patterns of corals can be expected.

Density plots of the numerical solutions of v component on one dimensional space shows some branching patterns when the parameters lie near the Hopf bifurcation line, $\alpha = \frac{\lambda^2}{\sqrt{\lambda-1}}$. Furthermore isosurfaces of the numerical solutions of v component on two dimensional space also shows some branching structures when appropriately chosen parameters, which lie in Turing space. These branching structures are somewhat similar to the branching structures of some branching corals (e.g. *Acropora* branching corals, *Montipora* branching corals etc.). The heterogeneity of the space patterns vary with the values of λ and α as well as the domain size.

REFERENCES

1. Castro P. & Huber M. (1997). *Marine Biology*. WCB/McGraw-Hill, USA.
2. Filatov M.V., Kaandorp J.A., Postma M., van Liere R., Kruszyski K. J., Ver-meij M.J., Streekstra G.J. & Bak R.P. (2010). A comparison between coral colonies of the genus *Madracis* and simulated forms. *Proceedings of the Royal Society B: Biological Sciences* **277**: 3555 – 3561. DOI: <http://dx.doi.org/10.1098/rspb.2010.0957>
3. Kaandorp J.A., Blom J.G., Verhoef J., Filatov M., Postma M. & M'uller W.E.G. (2008). Modelling genetic regulation of growth and form in a branching sponge. *Proceedings of the Royal Society B: Biological Sciences* **275**: 2569 – 2575. DOI: <http://dx.doi.org/10.1098/rspb.2008.0746>
4. Kaandorp J.A., Lowe C.P., Frenkel D. & Sloot P.M.A. (1996). Effect of nutrient diffusion and flow on coral morphology. *Physical Review Letters* **77**(11): 2328 – 2331. DOI: <http://dx.doi.org/10.1103/PhysRevLett.77.2328>
5. Kaandorp J.A., Sloot P.M.A., Merks R.M.H., Bak R.P.M., Vermeij M.J.A. & Maier C. (2005). Morphogenesis of the branching reef coral *Madracis mirabilis*. *Proceedings of the Royal Society B: Biological Sciences* **272**(1559): 127 – 133. DOI: <http://dx.doi.org/10.1098/rspb.2004.2934>
6. MathWorks (2014a). <http://www.mathworks.in/help/matlab/ref/pdepe.html>, Accessed on 04 April 2014.

7. MathWorks (2014b). <http://www.mathworks.in/help/matlab/ref/isosurface.html?searchHighlight=isosurface>, Accessed on 04 April 2014.
8. MathWorks (2014c). <http://www.mathworks.in/help/matlab/ref/isocaps.html?searchHighlight=isocaps>, Accessed on 04 April 2014.
9. Merks R.M.H. (2003). Branching growth in stony corals: a modelling approach. *PhD thesis*, Advanced School of Computing and Imaging, University of Amsterdam, The Netherlands.
10. Merks R.M.H., Hoekstra A.G., Kaandorp J.A. & Sloot P.M.A. (2003a). Diffusion-limited aggregation in laminar flows. *International Journal of Modern Physics C* **14**(9): 1171 – 1182.
DOI: <http://dx.doi.org/10.1142/S0129183103005297>
11. Merks R.M.H., Hoekstra A., Kaandorp J. & Sloot P. (2003b). Models of coral growth: spontaneous branching, compactification and laplacian growth assumption. *Journal of Theoretical Biology* **224**(2): 153 – 166.
12. Merks R.M.H., Hoekstra A., Kaandorp J. & Sloot P. (2003c). A problem solving environment for modelling stony coral morpho-genesis. *Lecture Notes in Computer Science* **2657**: 639 – 648.
DOI: http://dx.doi.org/10.1007/3-540-44860-8_66
13. Mistr S. & Bercovici D. (2003). A theoretical model of pattern formation in coral reefs. *Ecosystems* **6**: 61 – 74.
DOI: <http://dx.doi.org/10.1007/s10021-002-0199-0>
14. Murray J.D. (2003). *Mathematical Biology: Spatial Models and Biomedical Applications*, volume II. Springer-Verlag, Berlin Heidelberg, Germany.
15. Turing A.M. (1952). The chemical basis of morphogenesis. *Philosophical Transactions of the Royal Society of London* **237** (641): 37 – 72.